HHS Public Access

Author manuscript

J Alzheimers Dis. Author manuscript; available in PMC 2020 February 26.

Published in final edited form as:

J Alzheimers Dis. 2019 ; 67(3): 859–874. doi:10.3233/JAD-180871.

Paclitaxel Reduces Brain Injury from Repeated Head Trauma in Mice

Donna J. Cross[a,*], **James S. Meabon**[b,d], **Marcella M. Cline**[c,e], **Todd L. Richards**[f], **Amanda J. Stump**[a], **Chloe G. Cross**[a], **Satoshi Minoshima**[a], **William A. Banks**[c,g], **David G. Cook**[c,h]

[a]Department of Radiology and Imaging Sciences, University of Utah, Salt Lake City, UT, USA

[b]The Mental Illness Research Education and Clinical Center (MIRECC), and VA Puget Sound Health Care System, Seattle, WA, USA

[c]Geriatric Research Education and Clinical Center (GRECC) and VA Puget Sound Health Care System, Seattle, WA, USA

[d]Department of Psychiatry University of Washington, Seattle, WA, USA

[e]Department of Molecular and Cellular Biology, University of Washington, Seattle, WA, USA

[f]Department of Radiology, University of Washington, Seattle, WA, USA

[g]Department of Medicine, University of Washington, Seattle, WA, USA

[h]Department of Pharmacology, University of Washington, Seattle, WA, USA

Abstract

Repetitive mild traumatic brain injury (rmTBI) is known to disturb axonal integrity and may play an important role in the pathogenic cascades leading to neurodegeneration. One critical approach to reduce the future onset of neurodegeneration is to intervene in this process at an early stage following a brain injury. Previously we showed that direct application of the microtubule-stabilizing drug, *paclitaxel,* on the brain following controlled cortical impact improved motor function and reduced lesion size. Herein, we extended these findings to a model of mild brain injury induced by repeated closed-skull impacts. *Paclitaxel* was administered intranasally to circumvent its poor transport across the blood-brain barrier. Mice received five mild closed-skull impacts (one per day for five days). Intranasal *paclitaxel* was administered once only, immediately after the first impact. We found that *paclitaxel* prevented injury-induced deficits in a spatial memory task in a water tread maze. *In vivo* magnetic resonance imaging (MRI) and positron emission tomography with 18F-flurodeoxyglucose (FDG-PET) revealed that *paclitaxel* prevented structural injury and hypometabolism. On MRI, apparent, injury-induced microbleeds were observed in 100% of vehicle-treated rmTBI mice, but not in *paclitaxel*-treated subjects. FDG-PET revealed a 42% increase in whole brain glucose metabolism in paclitaxel-treated mice as compared to vehicle-treated rmTBI. Immunohistochemistry found reduced evidence of axonal injury and synaptic loss. Our results indicate that intranasal *paclitaxel* administration imparts neuroprotection

[*]Correspondence to: Donna J. Cross, PhD, Department of Radiology and Imaging Sciences, University of Utah, 30 N. 1900 E. #1A71, Salt Lake City, UT 84132-2140, USA. Tel.: +1 801 585 1346; d.cross@utah.edu.

Authors' disclosures available online (https://www.j-alz.com/manuscript-disclosures/18-0871r2).

against brain injury and cognitive impairment in mice. The results from this study support the idea that microtubule-stabilization strategies hold therapeutic promise in mitigating traumatic brain injury.

Keywords

Axonal injury; imaging; microtubule-stabilizing drug; repeat mild traumatic brain injury; synaptic preservation

INTRODUCTION

There is increasing evidence that repetitive mild traumatic brain injury (rmTBI) is associated with neurodegenerative disease [1-4]. Although the process by which rmTBIs lead to neurodegeneration is still under investigation, there is emerging evidence that loss of axonal integrity and cytoskeletal derangement may play a prominent role in the evolving pathogenic cascades that in later life can cause significant neurocognitive impairment [5-7]. One critical approach to reduce the future onset of neurodegeneration is to intervene in this process at an early stage following a brain injury. However, much work remains in the search for clinically effective pharmacological interventions to treat traumatic brain injury (TBI). Microtubules play a role in many homeostatic brain processes including cytoskeletal integrity and axonal transport, as well as in regulating cell morphology, proliferation, motility, and intracellular protein trafficking [8-11]. All of these processes may be disturbed by the primary mechanical insult in TBI [12]. In a previous study, we administered a microtubule-stabilizing (MT) drug, typically used to treat cancer, to mitigate acute head trauma [13].

Long used for chemotherapy to prevent mitosis in tumor cells, the prototypical, microtubule-stabilizing compound, *paclitaxel* has been well-studied in terms of binding and target characterization [14]. *Paclitaxel* prevents depolymerization by binding to β tubulin on the inner surface of microtubules [15, 16]. Studies have indicated that low doses of *paclitaxel* may be beneficial for acute CNS injuries, as well as neurological diseases [8, 17-21]. However, the neurotherapeutic potential of *paclitaxel* has been investigated only sparingly in models of focal neuronal injury [19, 20, 22, 23]. An *in vivo* rat study by Adlard et al. used intracortical delivery of *paclitaxel* after a penetrating needle stick injury and found reduced axonopathy and a preservation of MAP2 labeling in the injury area [22]. Another study showed that intrathecal administration of *paclitaxel* facilitated axonal regeneration in acute spinal cord injury in rats [19]. Sengottuvel et al. found *paclitaxel* promoted axonal growth *in vitro* and optic nerve regeneration after crush injury *in vivo* [20]. In addition, Ertürk et al. delivered *paclitaxel* to a dorsal root ganglion injury and found that the drug limited axonal retraction bulbs. This same study found that *paclitaxel* promoted axonal growth when applied *in vitro* to cultured neurons [23]. Collectively, these findings suggest that *paclitaxel* may be neurotherapeutic for focal neuronal injuries.

Previously we applied *paclitaxel* topically to the injury site in the brains of mice following a single, unilateral controlled cortical impact with craniotomy and found significant improvement in neurological function using “Catwalk” gait analysis [13]. This improvement corresponded to imaging biomarkers indicating reduced injury volume and edema, as well as

myelin preservation with *paclitaxel.* These encouraging results support the idea that acute TBI might benefit from treatment with *paclitaxel*. The aim of this present study was to determine if *paclitaxel c*ould mitigate repeated mild brain injury.

One significant challenge for the application of *paclitaxel* to brain injury is its low blood-brain barrier penetration when delivered systemically [24]. To address this issue and, more importantly, to limit systemic distribution and target specifically to the brain, we delivered *paclitaxel* via the intranasal (IN) route. IN administration for CNS drug delivery was proposed by Frey and colleagues more than two decades ago [25]. Our group has used IN administration as an alternative delivery approach in studies that included insulin for treatment of Alzheimer's disease (AD) [26], imaging agents such as manganese [27], and administration of hormones such as progesterone and testosterone [28, 29]. Brain uptake after IN administration is not dependent on classic distribution mechanisms. Research suggests that transport via IN administration is within the perivascular spaces of the brain, resulting in rapid distribution, which reaches steady state quickly [30, 31]. In this study, we assessed the pharmacokinetics of IN administration in mice using [3H]-*paclitaxel*.

To test the hypothesis that *paclitaxel* will prevent diffuse axonal injury from TBI, we utilized a mouse model with repeat mild TBI, which produced axonal injury in brain white matter and synaptic loss in the CA1 region of the hippocampus. We administered IN *paclitaxel* only one time after the first impact of a rmTBI protocol consisting of five impacts over five days without craniotomy. We tested the therapeutic efficacy of *paclitaxel* to mitigate injury-induced deficits with outcomes that included cognitive function on the radial water tread maze, imaging of structure and function using magnetic resonance imaging (MRI) and ^{18}F-flurodeoxyglucose positron emission tomography (FDG-PET) and immunohistochemistry.

MATERIALS AND METHODS

Subjects

All procedures and animal handling were conducted in accordance with the animal care guidelines issued by the National Institutes of Health and by the University of Washington Animal Care and Use Committee. For the rmTBI treatment and sham groups, adult male C57BL/6J mice were purchased from the Jackson Laboratory, Bar Harbor, ME, USA. Animals were kept on a 12-h light/12-h dark cycle with *ad libitum* access to food and water, and were randomly assigned to four groups: sham surgery with IN saline (n = 5), or IN *paclitaxel* (n = 3), repeat impact with IN saline (n = 9), or IN *paclitaxel* (n = 7). Statistical analyses of imaging and behavioral outcomes revealed no statistical differences or trends of differences between sham controls receiving saline or *paclitaxel* ($F[1, 6] = 0.010$, $p <= 0.922$, n.s.), so these groups were combined as a single control group (sham). For paclitaxel pharmacokinetic assessment, male CD-1 mice were purchased from Charles River, Wilmington, MA, USA and were kept on a 12-h light/12-h dark cycle with ad libitum access to food and water.

Intranasal paclitaxel pharmacokinetics

With a protocol similar to a previously published study [28], male CD-1 mice (8 weeks, n = 3–5 per time point) were anesthetized with urethane and administered 1 μl with 1,000,000 DPM tritium labeled paclitaxel (American Radiolabeled Chemicals, St. Louis, MO, USA) with unlabeled paclitaxel in PBS to equal 0.6 mg/kg (dose used in *in vivo* studies below). The radiolabeled paclitaxel was administered IN using a micropipette tip inserted 4 mm into the left nostril of each mouse. A subset of animals (n = 3, 20 min only) received intravenous (IV) administration (left jugular vein) of radiolabeled paclitaxel for brain/serum ratio quantification. At 10, 20, 40, or 60 min after administration, the carotid artery was exposed and blood taken. The mouse was then decapitated and the brain removed and dissected [32] on ice into 11 regions: olfactory bulb, occipital cortex, striatum, frontal cortex, hypothalamus, thalamus, hippocampus, parietal cortex, cerebellum, midbrain, and pons-medulla. Each region was weighed. Collected whole blood was allowed to clot at room temperature, centrifuged at 5400 g for 10 min at 4°C, and 50 μl of the resulting serum removed. Radioactivity in each of brain region and the matching serum sample was measured in a gamma counter (Perkin Elmer; Waltham, MA, USA) for 30 min. Percent injected dose in 1 ml of serum (%Inj/ml) was calculated by: %Inj/ml = [100*(CPM/ml)]/Inj (Inj = counts per minute (CPM) administered, CPM/ml = radioactivity in 1 ml of serum). Percent injected dose taken up per gram of brain region (%Inj/g) was calculated at each time point by: %Inj/g = [100*(CPM/R)](/Inj(W)) (W = weight of brain region in grams, CPM/R = radioactivity in brain region).

Repeat impact TBI and drug administration

Mice were anesthetized and maintained with isoflurane (1.5–2.5% in flowing O_2 at 2L/min) during surgery and core temperature was maintained at 37°C via paraffin heating pad. The mice were secured in a stereotaxic frame (Kopf Instruments, Tujunga, CA, USA), and the scalp depilated with topical cream diluted with saline (Nair; Church & Dwight Co. Inc., Ewing, NJ, USA). An impactor device (Impact One; Leica Biosystems, Buffalo Grove, IL, USA) was positioned directly above the midline of the skull between bregma and lambda and a mark was made with a permanent marker to ensure the same area was impacted daily. Mice received a mild closed-skull TBI or sham impact (anesthesia and treatments, no impact) once daily for five consecutive days (5 mm impact tip, 1 mm depth, 5 m/s velocity, 200 ms dwell time). Low-dose IN paclitaxel (0.0175 μmol of paclitaxel in 5 μl volume) or 5 μl saline (vehicle) was administered (2.5 μl in each naris) immediately after the initial impact, but not on subsequent days. Immediately following surgery, mice were removed from anesthesia, placed in a warmed recovery box, and given a subcutaneous injection of buprenorphine (0.5 mg/kg).

Outcome study design

The study protocol was designed to accommodate multiple endpoints, thus necessitating accommodations for logistical work flow and timing constraints of the experimenters. The injury paradigm of 5 impacts in 5 days was performed Monday-Friday. MRI imaging was conducted early (4 days) after the injury to assess if the injury protocol resulted in observable lesion on structural imaging. Maze testing requires a full week (M-F) for

acquisition plus short-term memory test as well as one more day of Friday testing the following week for the long-term memory. Since imaging requires anesthesia we did not plan any imaging experiments during the maze testing time frame, nor within 3 days prior to maze testing. Depending on the cohort size, FDG-PET requires 1–2 days and "hot" animals needed to be housed overnight in shielded housing then moved back to regular housing, therefore imaging could not be performed on a Friday. Euthanasia was performed within 1 week of the FDG-PET imaging.

Radial water tread maze (RWT)

Water maze testing began at 10 days after final impact. The full procedure and application to a mouse model of TBI has been published previously by our group [33]. This test requires no swimming, capitalizes on the natural tendency of mice to avoid open areas in favor of hugging the edges of an apparatus (thigmotaxis), and has been used successfully to distinguish TBI from sham mice previously [33, 34]. The RWT maze consists of a 32-inch galvanized steel tub with 9 holes placed at equal intervals around the device, roughly 1½ inch above the apparatus floor. Of these, 8 terminate after roughly 1 inch (decoy exits), and 1 leads to a safety box hidden behind a 90-degree angle bend to prevent visual confirmation of escape route. The safety box consists of a dark plastic container (30"L × 15"W × 15"H) heated externally via electronic heating pad. Five large unique visual cues line the sides of the apparatus for spatial orientation.

Testing was conducted in a brightly lit room. Before each mouse was tested, the maze was sanitized with 70% ethanol and filled with 1 inch of 12–14°C water. The temperature was monitored during filling to ensure it was within the desired range. After maze preparation, each mouse was placed in the center of the maze and given 180 s to find the escape hole. If the mouse was unable to find the escape within the time period, the mouse was gently guided by hand to the exit and the trial was recorded as 180 s. If a mouse attempted to enter a decoy hole and did not voluntarily re-enter the maze after 5 s, they were returned to the center of the maze by hand. Once inside the safety box, the mouse was presented with a high-reward food treat and allowed to remain in the box for 60 s. The safety box and maze were sprayed with 70% ethanol between trials to prevent olfactory cues. Each mouse was tested for three sequential trials, with an inter-trial interval of one minute. Water was then changed between mice, so each mouse was tested in fresh water. Mice were given 3 trials a day for 4 days (acquisition period), followed by a short-term memory test consisting of 3 trials on day five. Mice were then unexposed to the maze until day 12 (day 22 after final impact), at which they underwent 3 final trials (long-term memory test).

Imaging and image analysis

Magnetic resonance imaging (MRI), including diffusion tensor imaging (DTI), has been proposed as a biomarker to assess rmTBI clinically. We acquired MR imaging including T1-weighted, T2-mapping, and DTI at 4 days after the final impact. Mice were anesthetized with isoflurane and scanned on an ultra-high resolution 14T MRI (Avance III, Bruker BioSpin Corp, Billerica, MA). T1-weighted imaging to assess gross brain structure and obvious lesions, was acquired using a 3D Modified Driven Equilibrium Fourier Transform (MDEFT) sequence: voxel size: 0.14 × 0.14 × 0.25 mm^3, 64 slices, flip angle/repetition

time/echo time (FA/TR/TE): 121/5000 ms/1.9 ms. The presence of edema under the impact region was assessed by T2 quantitative mapping (T2) with a voxel size of 0.12 × 0.12 × 1.0 mm^3, 15 slices, TR 1/4 2000ms,16 echoes, spacing: 6.7 ms, TE Effective 1:6.7 ms, TE Effective 2:13.4 ms. DTI was acquired as a 4 shot echo planar image (EPI), TR/TE = 500/16.482 ms, 30 diffusion directions, Max bval = 6477.26849710899 s/mm^2, multislice 3d, FOV 22.4 × 22.4 × 22.4 mm, Matrix size= 112 × 80 × 82, time was 1h 35 min and 40 s. MR image sets including T1-weighted and T2 maps were manually inspected (DC) for the presence of anatomical abnormalities, edema and/or lesions resulting from the impact procedure. Manual inspection consisted of visual review of synchronized image sets through approximately 20 axial slices covering the area under impact region. During this manual inspection, it was noted that there were small lesions under the impact area in all of the saline-treated rmTBI subjects that were not present in the paclitaxel-treated mice.

DTI processing included the application of a custom algorithm running within the Neuroimaging Informatics Tools and Resources Clearinghouse (NITRC) DTIPrep software package (http://www.nitrc.org/projects/dtiprep/), which allows elimination of image frames contaminated by motion-derived artifacts, followed by eddy current and B0 corrections and confers several advantages. The resultant diffusivity maps had little spatial distortion, artifacts of subject motion or inhomogeneities of magnetic (B0) or RF fields; and showed a high degree of white/gray matter contrast. Fractional anisotropy (FA) maps are constructed from DTI by FSL software (Analysis Group, FMRIB, Oxford, UK) and compared between groups using FSL tract-based spatial statistics (TBSS). Manual regions of interest (ROI) analysis as well as left and right regions were hand-drawn by a blinded investigator over 3 consecutive slices as indicated and averaged.

Cerebral glucose activity was assessed at 31 days after last impact using ^{18}F-flurodeoxyglucose positron emission tomography (FDG-PET) (Inveon micro-PET; Siemens, Munich, Germany). PET imaging was performed under isoflurane anesthesia with 30 min uptake after 250 μCi intraperitoneal injection of FDG. High-resolution images were acquired over the whole brain for 30 min and processed using 3D OSEM/MAP reconstruction with a spatial resolution of approximately 1 mm. Given the limited spatial resolution of FDG-PET of the mouse brain, whole brain analysis (rather than region-based) was performed on standardized uptake values (SUV) calculated images using ImageJ software.

Immunostaining

Mice were euthanized using intraperitoneal ketamine/xylazine until respiratory arrest and then transcardially perfused with PBS followed by 4% formaldehyde. Brains were removed and postfixed overnight in 4% paraformaldehyde in PBS at 4°C, followed by 24 h in 20% sucrose in PBS, and then 24 h in 30% sucrose. Tissue was then paraffin embedded, cut coronally to 5 μm sections, and slide mounted. Sections were deparaffinized in xylenes (2 times at 10 min each), followed by 100% ethanol (2 times for 5 min each), 95% ethanol (once for 5 min), 70% ethanol (once for 5 min) and finally distilled H_2O (2 times for 5 min each). Tissues were permeabilized (1 h, room temperature, 0.2% Triton X-100 and 0.01% sodium azide in PBS) followed by three 5 min washes in PBS. Antigen retrieval was performed by heating at 80°C for 30 min in 50 mM sodium citrate (pH 8.5–9.0). Sections

were then cooled to room temperature, washed in PBS (3 times for 5 min each) and blocked in PBS with 10% normal goat serum (NGS) for 2 h at room temperature with gentle agitation on an orbital shaker (10 rpm). After circling individual tissue sections using a hydrophobic barrier pen, sections were covered with primary antibody solution (PBS, 5% NGS; 200 μl per section) and incubated at 4°C overnight at 1:1000 with rabbit mAb PSD-95 (Cell Signaling, Danvers, MA). Following a brief rinse and 3 PBS washes (each 10 min in duration) secondary antibodies were applied. Anti-rabbit/AF555 secondary antibody (Molecular Probes, Grand Island, NY) were applied to tissue sections for 3 h at room temperature, followed by three 10 min washes in PBS. Slides were lastly rinsed into water to remove buffer salts, mounted and cover slipped. Slides were mounted in Prolong gold anti-fade solution with DAPI (Life Technologies, Grand Island, NY, USA). Laser scanning confocal imaging was conducted using a Leica TCS SP2 confocal/multiphoton hybrid microscope with tunable emission gating and using sequential, between stack, single photon excitation at 488, 543, and 633. Z-plane images acquired the full volume thickness of each slice imaged (i.e., 50 μm for floating sections and 5 μm for paraffin-embedded sections) using system optimized stepping. Within an experiment, all directly compared sections/ slides were identically and simultaneously prepared.

Gallyas silver stain was used to detect axonal retraction bulbs. Gallyas method was performed using a commercial kit (FD Neurosilver Kit, FD Neurotechnologies, Inc. Columbia, MD, USA) and is characterized by its stability, reproducibility, and ability to visualize abundant deposits. This commonly used method allows reproducible examination for pathological deposits such as neurofibrillary tangles or glial cytoplasmic inclusions from TBI. Mouse brains were coronally sectioned between [Bregma: −3.4 and −2]. Samples were cut serially with each successive tissue slice being placed onto the next microscope slide. Anatomically-matched tissue sections from 2–4 members of each group were represented on each slide to ensure that each group was well-matched in terms of anatomy and received equal downstream processing treatment. Random planes relative to Bregma were examined and all subjects were matched to the selected plane. Slides were stained together as a full group using the FD Neurosilver Kit according to the manufacturer’s instructions. Slides from all study conditions were simultaneously processed, darkened for ~3 min at room temperature and stopped in parallel. After development, slides were coverslipped. Using brightfield microscopy, the entire surface of each tissue slice was briefly examined for argyrophilic degeneration. Due to a lack of notable staining elsewhere, quantitation of retraction bulbs was determined in the dorsal hippocampal commissure / corpus collossum / alveus inferior to the site of TBI and proximal (superior) to where the PSD-95 micrographs in Fig. 6 were taken. A total of two slices per animal were examined from two separate silver-stained preparations.

PSD-95 expression was indirectly quantified using the histogram function of Adobe Photoshop to determine the PSD-95-positive immunofluorescence (i.e., green channel only; mean ± standard deviation) within matched ROIs. The ROIs used for statistical analyses are indicated by a white box for each subject in Fig. 6.

Statistical analysis

Where appropriate, one-factor between-group ANOVAs or Student *T* tests were used to compare paclitaxel-rmTBI to Sham or saline-rmTBI groups. All reported *p* values were based upon two-tailed critical values ($p \leq 0.05$). Radial water tread maze data were analyzed by two-way analysis of variance (ANOVA) with training or test days as a repeated measures within-subjects factor and treatment (drug/no drug) as a between-subjects factor. Following ANOVA the a priori hypothesis that injured/untreated groups would be statistically significantly different from both vehicle/sham-treated and injured/paclitaxel-treated groups was performed using a Helmert individual comparisons test [35, 36]. PK data for time versus %Inj/g brain tissue were analyzed by two-way ANOVA. Statistical analyses were carried out using SPSS software (IBM, Armonk, NY, USA).

RESULTS

Pharmacokinetics of [3H] Paclitaxel in the brain after intranasal administration

We first assessed the pharmacokinetics of [3H]-paclitaxel after IN administration at a dose of 0.0175 μmol (0.6 mg/kg for 25 g mice). Inspection of the time activity curves in several brain regions (Fig. 1A) indicated that overall, [3H]-paclitaxel concentration in the brain remained fairly stable over the interval of 10–60 min. However, there were different levels of [3H]-paclitaxel uptake among the 11 brain regions analyzed. This was confirmed by a two-factor ANOVA where the time factor was not statistically significant ($F[3, 30] = 2.583$, n.s.) and the brain region factor was statistically significant ($F[1, 30] = 59.36$, $p < 0.00001$). Brain region differences in [3H]-paclitaxel uptake at 20 min post injection are further illustrated in Fig. 1B. As expected olfactory bulb uptake was higher than other brain regions [28]. Interestingly, uptake was also comparatively high in the striatum and hypothalamus, which is unique for paclitaxel. We also assessed [3H]-paclitaxel distribution in peripheral organs. Only 0.3% Inj/ml was found in serum and 2% injected dose/g-tissue in the kidney (2.06 ± 1.8, 0.66 ± 0.7, 0.30 ± 0.2, and 0.02 ± 0.0, mn ± sd of %Inj/ml of [3H]-paclitaxel, in kidney, liver, serum and urine, respectively). Taken together these results demonstrate that paclitaxel delivered IN is taken by multiple brain regions at levels that remain stable for at least 60 min.

Paclitaxel prevents white matter injury from repeat mild impacts

Diffusion tensor images were acquired in all subjects, however due to a coil malfunction, we were unable to acquire usable artifact-free FA maps in 5 of 7 paclitaxel-treated subjects. In the remaining subjects of the saline-treated rmTBI and sham groups, the FA maps were assessed on a voxel-wise basis using tract-based spatial statistics (TBSS). The rmTBI group had extensive regions of decreased FA throughout the white matter tracts of the brain, in particular the external capsule, fimbria of the hippocampus, the ventral hippocampal commissure, and the corpus callosum (Fig. 2A). This voxel-based analysis was confirmed by manual region of interest analysis. Manual ROI indicated that rmTBI resulted in decreased FA in the external capsule (green arrows) at 4 days after final impact (17% (0.21 ± 0.01 versus 0.25 ± 0.01, unpaired *t*-test $p \leq 0.01$) as compared to sham mice (Fig. 2B). These imaging results were used to define the location of the post-mortem immunohistochemistry. At 45 days after rmTBI, a corresponding post-mortem examination of the external capsule

using Gallyas silver stain confirmed *in vivo* imaging findings of diffuse axonal injury. More importantly, we were able to assess the white matter histologically in the paclitaxel-treated subjects. Argyrophilic axonal degeneration is seen in cortical white matter of the alveus/external capsule in 5 of 6 saline-treated rmTBI mice with varicosities (bilateral, and at least 1 argyrophilic bulb per side observed). One mouse had very prominent degeneration (15 argyrophilic bulbs in a single field in the dorsal hippocampal commissure / corpus collossum). 1 of 5 sham mice had a single unilateral, translucent bulb which is likely artifactual. However, to favor a conservative assessment it was counted as a bona fide argyrophilic retraction bulb. 0 of 3 paclitaxel-treated sham mice had evidence of argyrophilic degeneration in any region. 0 of 5 paclitaxel-treated rmTBI mice had at least 1 argyrophilic retraction bulb in the white matter regions within, or contiguous with, the alveus. However, in 2 of 5 paclitaxel-treated rmTBI treated mice argyrophilic degeneration was observed in the area consisting of the external capsule, brachium of the superior colliculus, and the optic tract (Fig. 2C).

Paclitaxel administration prevents apparent microbleed

In the same imaging session at 4 days after final impact, T1-weighted (T1-w) images and T2 maps were acquired to reveal any gross anatomical injury and/or edema. Manual inspection consisted of visual review of synchronized image sets through approximately 20 axial slices covering the area under impact region. During this manual inspection, it was noted that there were small lesions under the impact area in all of the saline-treated rmTBI subjects that were not present in any slices of either MR acquisition of the paclitaxel-treated mice. A likely tissue strain microhemorrhage was observed in the cortical region directly below the impact area (Fig. 3A). This lesion was found in 100% (9/9) of rmTBI mice receiving saline-only treatments and no paclitaxel-treated mice (0%, 0/6, one PTX subject MRI had a slight artifact in the region of the impact therefore it was not possible to definitively conclude no lesion) showed evidence of the injury (Fig. 3B). This defect resolved by time of euthanasia/immunohistology, so pathologic confirmation of the microbleed was not performed.

Spatial memory impairment from repeat mild impacts is prevented by paclitaxel

Mice were tested at ten days after final impact for spatial memory impairment using a radial water tread (RWT) maze, which was developed specifically to test spatial memory in mice [33, 37]. A two-way ANOVA (Days 1–12, between and within subjects factors, respectively) indicated that there was not a statistically significant difference between sham-saline versus sham-paclitaxel mice for either testing day, or the acquisition phase ($F[1, 6] = 0.010$, $p \leq 0.922$, n.s). Therefore, in further analyses these two sham groups were pooled. As shown in Fig. 4A, a two-way ANOVA (Days1–4) comparing Shams, rmTBI paclitaxel-treated, and rmTBI saline-treated animals revealed an overall statistically significant difference between groups ($F[2, 20] = 3.903$, $p \leq 0.037$), indicating that paclitaxel treatment significantly improved learning of the water tread maze by mice with repetitive mTBI. In keeping with this, a Helmert a priori individual comparisons test [36] further confirmed that vehicle-treated rmTBI mice performed significantly worse than the paclitaxel-treated rmTBI and sham groups ($p \leq 0.014$) and that the paclitaxel-treated rmTBI group performance was not significantly different from non-injured sham controls ($p \leq 0.324$, n.s.). In addition, Fig. 4B shows that RWT performance on post-exposure (sham or mTBI) mice at Days 5 and 12 also

showed that paclitaxel significantly reduced escape latencies, indicative of improved performance (F[2, 20] = 7.254, $p \leq 0.004$ and F[2, 20] = 4.595, $p \leq 0.023$; Day 5 and Day 12, respectively). Finally, an overall two-way ANOVA (treatment X Days; between and within subjects factors, respectively) encompassing Days 1–12 further confirmed that paclitaxel significantly reduced injury-induced deficits on the RTW maze (Day 5:24.2 ± 15.7 versus 69.78 ± 70.5 and Day 12:26.58 ± 21.4 versus 68.33 ± 50.16, mn ± sd, paclitaxel-rmTBI versus saline-rmTBI, respectively, F[1, 20] = 12.423, $p \leq 0.001$).

Paclitaxel preserves cerebral glucose metabolic activity and prevents synaptic loss from rmTBI

An alternative imaging modality used to investigate TBI in humans is FDG-PET, which assesses the metabolic activity associated with glucose uptake in the brain. Our group has previously reported regional metabolic deficits in Veterans years after mild repetitive blast TBIs using FDG-PET [38-40]. In our current study, mice underwent FDG-PET imaging at 31 days post rmTBI. Brain-injured mice showed significantly decreased whole brain FDG uptake, which was not observed in brain-injured mice receiving IN paclitaxel (Fig. 5). Whole brain standardized uptake values (SUV, pseudo-quantitative assessment of FDG-PET, dimensionless) were 120.5 ± 30.1, 90.3 ± 18.7, and 129.2 ± 23.0, mn ± sd for sham, saline, and paclitaxel (PTX), respectively, which is 43% increased in mice treated with paclitaxel as compared to saline (One-way ANOVA, $p = 0.0154$, F(2,17) = 5.386). Glucose consumption in the brain is associated with synaptic activity [41]. Since synapses are also supported by microtubule structural components, we further reasoned that paclitaxel could maintain post-synaptic regions in the hippocampus. Therefore, we examined synaptic density in the CA1 hippocampi after rmTBI (45 days) by immunostaining postsynaptic density-95 (PSD-95) protein, which is a well-established synaptic marker [42]. Figure 6 shows that overall PSD-95 immunostaining intensity was reduced in saline-treated mice exposed to rmTBI, while paclitaxel administration blocked the TBI-induced loss in PSD-95 immunostaining intensity. We also quantified PSD-95 expression in the demarked regions shown in Fig. 6 (mean PSD-95 immunostaining intensity (relative units) = 23.5 ± 3.7 s.e.m., 46.5 ± 7.7 s.e.m., and 47.6 ± 6.9 s.e.m.; corresponding to the saline/rmTBI, saline/Sham, and PTX/rmTBI, respectively; overall F[2, 6] = 4.62,$p \leq 0.06$; $N = 3$ for each group). Confirming the specific hypothesis that paclitaxel would restore injury-induced PSD-95 expression to saline-treated sham control levels, a Helmert a priori planned comparison test revealed that PSD-95 levels were significantly lower ($p \leq 0.023$) in the saline/rmTBI group compared to ± saline/Shams and PTX/rmTBI animals; and that there was no significant difference ($p > 0.90$, n.s.) in PSD-95 levels among the PTX-treated rmTBI animals compared to the saline/Sham group. This conclusion was further confirmed with separate hypothesis-independent *post-hoc* paired comparisons (saline/rmTBI versus saline/Sham, $p \leq 0.04$; saline/rmTBI versus PTX/rmTBI, $p \leq 0.04$; PTX/rmTBI versus saline/Sham, $p \leq 0.91$, n.s.).

These data support that paclitaxel reduces overall PSD-95 loss induced by rmTBI and also lends support to our FDG-PET findings (Fig. 5), in that synapse activity is associated with glucose consumption [41]. Taken collectively, the findings in this report argue that microtubule stabilization can provided protection against mild repetitive TBI that is reflected

at the anatomical structural and functional level, as well as by improved cognitive performance.

DISCUSSION

In this report, we demonstrate that IN *paclitaxel* treatment delivered after the first impact of a multi-impact model of repeat mild brain injury prevented axonal injury in mice. This finding was supported by improved spatial memory, preserved post-synaptic density in the CA1 hippocampus, and *in vivo* imaging that indicated structural and metabolic outcomes similar to sham subjects. To our knowledge, this is the first evidence that this therapeutic strategy can mitigate structural and functional impairments from repeated mild TBI. Although the use of microtubule-stabilizers has been proposed for neurotherapeutic uses, including AD disease and other tauopathies, this approach has been limited to models of focal axonal injury. Previous studies have focused specifically on the potential of microtubule-stabilizers to maintain axonal function and structure [19-23]. Synaptic loss is a well-described feature of many animal models of brain injury [43], as well as in clinical TBI [21, 44-47]. A previous study by Erez et al found *paclitaxel* rescued tau-induced decreases in synaptic transmission *in vitro* [48]. However, the focus was on presynaptic vesicle release and alterations in excitatory postsynaptic potential amplitude and did not look specifically at post-synaptic density. Preservation of post-synaptic density may simply be explained by prevention of deafferentation from axonal loss or may be a direct effect of *paclitaxel*-microtubule stabilization on dendrites, which could not be distinguished in the current study.

We found significant improvement in spatial memory and increased FDG brain uptake measured by PET imaging in mice treated with a single dose of *paclitaxel*. These results are consistent with findings that FDG uptake in the brain is generally associated with brain activity [49, 50]. Numerous clinical studies, including those from our group examining Veterans with repetitive blast-related rmTBI, and others of mild impact TBI have indicated decreased FDG uptake on PET imaging [38-40, 51, 52]. Therefore, the finding that our mouse model of rmTBI model resulted in significantly decreased brain FDG uptake, at one month after the injury, is translationally consistent with human studies. Although infection and inflammation are known to increase FDG uptake on PET images, [53] research suggests that the neuroinflammation specifically may contribute less to overall brain FDG-PET uptake than brain activity [54]. The spatial memory preservation seen in mice treated with *paclitaxel* is a novel finding. Although it has been proposed that microtubules may be involved in learning and memory processes, the mechanism of action is not yet fully understood [55]. In 2006, insulin, delivered via the IN route, was shown to improve memory in patients with memory impairment [56]. A subsequent study by the same group indicated increased brain uptake of FDG in amnestic cognitive impairment after IN insulin [26]. In a more recent study, IN insulin improved memory and decreased neuroinflammation in a model of traumatic brain injury [57]. Although it is beyond the scope to this study to determine the exact mechanism by which IN *paclitaxel* preserved brain FDG uptake as well as spatial memory, we may also speculate that these effects could be attributed to modulation of brain energetics. Further studies on effect of *paclitaxel* to preserve memory function in TBI and other neurological conditions are warranted.

The prevention of the injury-induced cortical lesion, possibly a microbleed, after administration of *paclitaxel* was not anticipated. However, our previous research applying *paclitaxel* directly to the site of controlled cortical impact found a significant reduction in injury volume and edema [13]. Hemorrhage is a common feature in moderate to severe TBI [58]. Microbleeds, observed in acute TBI, are a result of vascular damage. The detection of microbleeds after mild TBI is an area of considerable clinical research effort [59-61]. In our study we only acquired MR imaging at 4 days after the final impact, therefore we do not know if *paclitaxel* administration after the first impact completely prevented the lesion, or facilitated tissue recovery. However, this finding raises intriguing possibilities for the application of microtubule-stabilizers to more severe trauma where hemorrhage is a serious complication [62]. Also, because the imaging took place at 4 days after impact, and the mice were not euthanized until 45 days it was not possible to confirm histologically that the post-injury lesion was actually a microbleed. This finding will be further investigated in future research.

The pharmacokinetics of IN *paclitaxel* delivery indicated a brain uptake of 0.08–0.23 %injection/g brain tissue. These values convert to a tissue concentration of 14–40 pmol/g of brain tissue. For kidney, 2% uptake of the administered dose would give a tissue concentration of about 350 pmol/g of tissue. These biologic effects, despite low brain uptake are consistent with previous research of other small molecules [28, 29]. Although MT-stabilizers including *paclitaxel* may be neurotoxic at doses required to treat cancer [63], other research indicates an opposite (neurotherapeutic) effect of *paclitaxel* in lower concentrations and doses. An *in vivo* study with intracortical delivery of 853.9 ng *paclitaxel* after penetrating needle injury found reduced axonopathy [22]. Another showed that 256 ng/day via intrathecal administration facilitated axon regeneration in acute spinal cord injury in rats [19]. In another study, 8.54 ng *paclitaxel* delivered to a dorsal root ganglion injury limited axonal retraction bulbs, while in the same study, only 10 nM applied *in vitro* to cultured neurons promoted axonal growth [23]. Sengottuvel et al. found 3 nM *paclitaxel* promoted axon growth *in vitro* and 4.27 ng promoted optic nerve regeneration *in vivo* [20]. Collectively, these findings along with those from our study suggest that low dose *paclitaxel* is neurotherapeutic. In fact, the finding that *paclitaxel* can be neurotherapeutic at low doses and neurotoxic at higher ones, should not be surprising. Medical practice has many examples of therapeutics, from botulimun toxin to acetaminophen, that have a range of beneficial effects despite high dose toxicity.

One advantage to IN delivery is that using a commercially available drug delivery device [64], a drug can be quickly administered to injured patients by medical personnel (from the sidelines of football and hockey games, or in the military field) under up-tempo conditions (i.e., light weight and without requiring refrigeration, electricity, or sophisticated administration equipment). Some skepticism for IN drug delivery remains within the field of central nervous system drug development, particularly with respect to translation of results from mouse studies to human. Main objections include: the mouse brain is diminutive and diffusion distances are shorter than in humans, and the olfactory bulb of the mouse is large compared to that of the human so it is not surprising that mice have drug uptake via the olfactory nerve tract. The success of IN insulin as a therapeutic for AD, argues against these concerns [26]. Also, and more directly, distribution of substances into the brain after IN

administration is not dependent on classic brain distribution mechanisms. Instead, distribution is very rapid, reaches steady state quickly, and is fairly stable over one hour [64]. The exact mechanism of action is still not entirely clear, however. It has been suggested that transport after IN administration is within the perivascular space of the brain [30, 31].

This study has some limitations. First, a coil malfunction that was not apparent at the time of imaging and did not compromise the other imaging acquisitions (T1 w and T2 mapping), was discovered after the study was completed. The malfunction affected the quality of the DTI, particularly in the middle of the brain and we were unable to analyze the FA maps from the *paclitaxel*-treated group that were acquired at 4 days post-injury. However, we applied silver stain of the external capsule at 45 days for all subjects, which showed no evidence of axonal injury in *paclitaxel*-treated mice. We also examined the *in vivo* structural T1-weighted and T2 mapping and confirmed that *paclitaxel*-treated subjects did not have overt brain lesions at the 4 days time point. Second, the neuropathological evidence of synaptic preservation based on PSD-95 stain is considered preliminary and support for this finding will be investigated in future studies using electron microscopy. Third, we do not know the temporal dynamics for repeat mild impacts on cytoskeletal derangements and the maximum interval during which the administration of microtubule-stabilizers will mitigate impairments. In this study we administered the drug immediately following the first impact. In future studies, we will determine future translational potential of microtubule-stabilizing therapeutics by providing insight into the temporal dynamics related to delivery. Lastly, only male mice were used in this study. Research is underway to investigate sex differences in the rmTBI model as well as response to *paclitaxel* treatment.

Conclusions

We found that *paclitaxel* treated mice did not suffer from the spatial memory impairment seen in the vehicle-only rmTBI mice. *In vivo* imaging of treated mice revealed preservation of glucose uptake on FDG-PET and no significant differences as compared to sham mice in white matter integrity on DTI. Apparent micro-hemorrhage seen on imaging in vehicle treated mice was not observed in *paclitaxel*-treated mice. Postmortem examination of *paclitaxel*-treated brains confirmed *in vivo* imaging results. In particular, we found no indication of axonal injury after treatment, and, more importantly, *paclitaxel* protected against synaptic loss in the CA1 region of the hippocampus. These results indicate that microtubule-stabilizers, more specifically *paclitaxel*, may be neuroprotective against repeated mild brain injury.

ACKNOWLEDGMENTS

The authors would like to thank Greg Garwin and Bradley Neal for their assistance with the research in this study. Support for this research was provided by the Institute for Translational Health Sciences pilot grant UL1TR000423 (D.J.C.) and the University of Washington Center on Human Development and Disability small animal imaging and behavioral cores (HD 083091). These studies were supported by R01AG046619 (W.A.B.), Department of Veterans Affairs Office of Research and Development Medical Research Service RDIS# 0005 (D.G.C.), VA Puget Sound Health Care System Seed Grant (J.S.M.) University of Washington Friends of Alzheimer's Research (D.G.C), University of Washington Royalty Research Fund (D.G.C.).

REFERENCES

[1]. Daneshvar DH, Goldstein LE, Kiernan PT, Stein TD, McKee AC (2015) Post-traumatic neurodegeneration and chronic traumatic encephalopathy. Mol Cell Neurosci 66, 81–90. [PubMed: 25758552]

[2]. McKee AC, Cairns NJ, Dickson DW, Folkerth RD, Keene CD, Litvan I, Perl DP, Stein TD, Vonsattel JP, Stewart W, Tripodis Y, Crary JF, Bieniek KF, Dams-O'Connor K, Alvarez VE, Gordon WA, group TC (2016) The first NINDS/NIBIB consensus meeting to define neuropathological criteria for the diagnosis of chronic traumatic encephalopathy. Acta Neuropathol 131, 75–86. [PubMed: 26667418]

[3]. Omalu BI, DeKosky ST, Minster RL, Kamboh MI, Hamilton RL, Wecht CH (2005) Chronic traumatic encephalopathy in a National Football League player. Neurosurgery 57, 128–134; discussion 128–134.

[4]. McKee AC, Cantu RC, Nowinski CJ, Hedley-Whyte ET, Gavett BE, Budson AE, Santini VE, Lee HS, Kubilus CA, Stern RA (2009) Chronic traumatic encephalopathy in athletes: Progressive tauopathy after repetitive head injury. J Neuropathol Exp Neurol 68, 709–735. [PubMed: 19535999]

[5]. Sundman MH, Hall EE, Chen NK (2014) Examining the relationship between head trauma and neurodegenerative disease: A review of epidemiology, pathology and neuroimaging techniques. J Alzheimers Dis Parkinsonism 4, 137. [PubMed: 25324979]

[6]. Henry LC, Tremblay S, Boulanger Y, Ellemberg D, Lassonde M (2010) Neurometabolic changes in the acute phase after sports concussions correlate with symptom severity. J Neurotrauma 27, 65–76. [PubMed: 19761385]

[7]. Henry LC, Tremblay S, De Beaumont L (2017) Long-term effects of sports concussions: Bridging the neurocognitive repercussions of the injury with the newest neuroimaging data. Neuroscientist 23, 567–578. [PubMed: 27188455]

[8]. Brunden KR, Lee VM, Smith AB 3rd, Trojanowski JQ, Ballatore C (2017) Altered microtubule dynamics in neurodegenerative disease: Therapeutic potential of microtubule-stabilizing drugs. Neurobiol Dis 105, 328–335. [PubMed: 28012891]

[9]. Etienne-Manneville S (2004) Actin and microtubules in cell motility: Which one is in control? Traffic 5, 470–477. [PubMed: 15180824]

[10]. Geisert EE Jr, Johnson HG, Binder LI (1990) Expression of microtubule-associated protein 2 by reactive astrocytes. Proc Natl Acad Sci U S A 87, 3967–3971. [PubMed: 1692628]

[11]. Takamiya Y, Kohsaka S, Toya S, Otani M, Tsukada Y (1988) Immunohistochemical studies on the proliferation of reactive astrocytes and the expression of cytoskeletal proteins following brain injury in rats. Brain Res 466, 201–210. [PubMed: 3359311]

[12]. Smith DH, Hicks R, Povlishock JT (2013) Therapy development for diffuse axonal injury. J Neurotrauma 30, 307–323. [PubMed: 23252624]

[13]. Cross DJ, Garwin GG, Cline MM, Richards TL, Yarnykh V, Mourad PD, Ho RJ, Minoshima S (2015) Paclitaxel improves outcome from traumatic brain injury. Brain Res 1618, 299–308. [PubMed: 26086366]

[14]. Fernandez-Peralbo MA, Priego-Capote F, Luque de Castro MD, Casado-Adam A, Arjona-Sanchez A, Munoz-Casares FC (2014) LC-MS/MS quantitative analysis of paclitaxel and its major metabolites in serum, plasma and tissue from women with ovarian cancer after intraperitoneal chemotherapy. J Pharm Biomed Anal 91, 131–137. [PubMed: 24447964]

[15]. Amos LA, Lowe J (1999) How Taxol (R) stabilises microtubule structure. Chem Biol 6, R65–R69. [PubMed: 10074470]

[16]. Diaz JF, Barasoain I, Andreu JM (2003) Fast kinetics of Taxol binding to microtubules. Effects of solution variables and microtubule-associated proteins. J Biol Chem 278, 8407–8419. [PubMed: 12496245]

[17]. Brunden KR, Yao Y, Potuzak JS, Ferrer NI, Ballatore C, James MJ, Hogan AM, Trojanowski JQ, Smith AB 3rd, Lee VM (2011) The characterization of microtubule-stabilizing drugs as possible therapeutic agents for Alzheimer's disease and related tauopathies. Pharmacol Res 63, 341–351. [PubMed: 21163349]

[18]. Lou K, Yao Y, Hoye AT, James MJ, Cornec AS, Hyde E, Gay B, Lee VM, Trojanowski JQ, Smith AB 3rd, Brunden KR, Ballatore C (2014) Brain-penetrant, orally bioavailable microtubule-stabilizing small molecules are potential candidate therapeutics for Alzheimer's disease and related tauopathies. J Med Chem 57, 6116–6127. [PubMed: 24992153]

[19]. Hellal F, Hurtado A, Ruschel J, Flynn KC, Laskowski CJ, Umlauf M, Kapitein LC, Strikis D, Lemmon V, Bixby J, Hoogenraad CC, Bradke F (2011) Microtubule stabilization reduces scarring and causes axon regeneration after spinal cord injury. Science 331, 928–931. [PubMed: 21273450]

[20]. Sengottuvel V, Leibinger M, Pfreimer M, Andreadaki A, Fischer D (2011) Taxol facilitates axon regeneration in the mature CNS. J Neurosci 31, 2688–2699. [PubMed: 21325537]

[21]. Ballatore C, Brunden KR, Trojanowski JQ, Lee VM, Smith AB 3rd (2017) Non-naturally occurring small molecule microtubule-stabilizing agents: A potential tactic for CNS-directed therapies. ACS Chem Neurosci 8, 5–7. [PubMed: 28095679]

[22]. Adlard PA, King CE, Vickers JC (2000) The effects of taxol on the central nervous system response to physical injury. Acta Neuropathol 100, 183–188. [PubMed: 10963366]

[23]. Erturk A, Hellal F, Enes J, Bradke F (2007) Disorganized microtubules underlie the formation of retraction bulbs and the failure of axonal regeneration. J Neurosci 27, 9169–9180. [PubMed: 17715353]

[24]. Amin ML (2013) P-glycoprotein inhibition for optimal drug delivery. Drug Target Insights 7, 27–34. [PubMed: 24023511]

[25]. Thorne RG, Emory CR, Ala TA, Frey WH 2nd (1995) Quantitative analysis of the olfactory pathway for drug delivery to the brain. Brain Res 692, 278–282. [PubMed: 8548316]

[26]. Craft S, Baker LD, Montine TJ, Minoshima S, Watson GS, Claxton A, Arbuckle M, Callaghan M, Tsai E, Plymate SR, Green PS, Leverenz J, Cross D, Gerton B (2012) Intranasal insulin therapy for Alzheimer disease and amnestic mild cognitive impairment: A pilot clinical trial. Arch Neurol 69, 29–38. [PubMed: 21911655]

[27]. Cross DJ, Minoshima S, Anzai Y, Flexman JA, Keogh BP, Kim Y, Maravilla KR (2004) Statistical mapping of functional olfactory connections of the rat brain *in vivo*. Neuroimage 23, 1326–1335. [PubMed: 15589097]

[28]. Banks WA, Morley JE, Niehoff ML, Mattern C (2009) Delivery of testosterone to the brain by intranasal administration: Comparison to intravenous testosterone. J Drug Target 17, 91–97. [PubMed: 19089688]

[29]. Ducharme N, Banks WA, Morley JE, Robinson SM, Niehoff ML, Mattern C, Farr SA (2010) Brain distribution and behavioral effects of progesterone and pregnenolone after intranasal or intravenous administration. Eur J Pharmacol 641, 128–134. [PubMed: 20570588]

[30]. Lochhead JJ, Wolak DJ, Pizzo ME, Thorne RG (2015)Rapid transport within cerebral perivascular spaces underlies widespread tracer distribution in the brain after intranasal administration. J Cereb Blood Flow Metab 35, 371–381. [PubMed: 25492117]

[31]. Lochhead JJ, Thorne RG (2012) Intranasal delivery of biologics to the central nervous system. Adv Drug Deliv Rev 64, 614–628. [PubMed: 22119441]

[32]. Glowinski J, Iversen LL (1966) Regional studies of catecholamines in the rat brain. I. The disposition of [3H]norepinephrine, [3H]dopamine and [3H]dopa in various regions of the brain. J Neurochem 13, 655–669. [PubMed: 5950056]

[33]. Cline MM, Yumul JC, Hysa L, Murra D, Garwin GG, Cook DG, Ladiges WC, Minoshima S, Cross DJ (2017) Novel application of a Radial Water Tread maze can distinguish cognitive deficits in mice with traumatic brain injury. Brain Res 1657, 140–147. [PubMed: 27923635]

[34]. Cline MM, Ostlie MA, Cross CG, Garwin GG, Minoshima S, Cross DJ (2017) Assessing spatial memory impairment in a mouse model of traumatic brain injury using a radial water tread maze. J Vis Exp, doi: 10.3791/55986.

[35]. Field A, Miles J, Field Z(2012) Discovering Statistics Using R, SAGE Publications.

[36]. Winer BJ, Brown DR, Michels KM (1991) Statistical Principles in Experimental Design, McGraw-Hill.

[37]. Pettan-Brewer C, Touch DV, Wiley JC, Hopkins HC, Rabinovitch PS, Ladiges WC (2013) A novel radial water tread maze tracks age-related cognitive decline in mice. Pathobiol Aging Age Relat Dis 3, doi: 10.3402/pba.v3i0.20679

[38]. Meabon JS, Huber BR, Cross DJ, Richards TL, Minoshima S, Pagulayan KF, Li G, Meeker KD, Kraemer BC, Petrie EC, Raskind MA, Peskind ER, Cook DG (2016) Repetitive blast exposure in mice and combat veterans causes persistent cerebellar dysfunction. Sci Transl Med 8, 321ra326.

[39]. Peskind ER, Petrie EC, Cross DJ, Pagulayan K, McCraw K, Hoff D, Hart K, Yu CE, Raskind MA, Cook DG, Minoshima S (2011) Cerebrocerebellar hypometabolism associated with repetitive blast exposure mild traumatic brain injury in 12 Iraq war Veterans with persistent post-concussive symptoms. Neuroimage 54 (Suppl 1), S76–82. [PubMed: 20385245]

[40]. Petrie EC, Cross DJ, Yarnykh VL, Richards T, Martin NM, Pagulayan K, Hoff D, Hart K, Mayer C, Tarabochia M, Raskind MA, Minoshima S, Peskind ER (2014) Neuroimaging, behavioral, and psychological sequelae of repetitive combined blast/impact mild traumatic brain injury in Iraq and Afghanistan war veterans. J Neurotrauma 31, 425–436. [PubMed: 24102309]

[41]. Sokoloff L, Reivich M, Kennedy C, Des Rosiers MH, Patlak CS, Pettigrew KD, Sakurada O, Shinohara M (1977) The [14C]deoxyglucose method for the measurement of local cerebral glucose utilization: Theory, procedure, and normal values in the conscious and anesthetized albino rat. J Neurochem 28, 897–916. [PubMed: 864466]

[42]. Kim E, Sheng M (2004) PDZ domain proteins of synapses. Nat Rev Neurosci 5, 771–781. [PubMed: 15378037]

[43]. Carbonell WS, Grady MS (1999) Regional and temporal characterization of neuronal, glial, and axonal response after traumatic brain injury in the mouse. Acta Neuropathol 98, 396–406. [PubMed: 10502046]

[44]. Gao X, Deng P, Xu ZC, Chen J (2011) Moderate traumatic brain injury causes acute dendritic and synaptic degeneration in the hippocampal dentate gyrus. PLoS One 6, e24566. [PubMed: 21931758]

[45]. Ojo JO, Bachmeier C, Mouzon BC, Tzekov R, Mullan M, Davies H, Stewart MG, Crawford F (2015) Ultrastructural changes in the white and gray matter of mice at chronic time points after repeated concussive head injury. J Neuropathol Exp Neurol 74, 1012–1035. [PubMed: 26360375]

[46]. Brody DL, Benetatos J, Bennett RE, Klemenhagen KC, MacDonald CL (2015) The pathophysiology of repetitive concussive traumatic brain injury in experimental models; new developments and open questions. Mol Cell Neurosci 66, 91–98. [PubMed: 25684677]

[47]. Harish G, Mahadevan A, Pruthi N, Sreenivasamurthy SK, Puttamallesh VN, Keshava Prasad TS, Shankar SK, Srinivas Bharath MM (2015) Characterization of traumatic brain injury in human brains reveals distinct cellular and molecular changes in contusion and pericontusion. J Neurochem 134, 156–172. [PubMed: 25712633]

[48]. Erez H, Shemesh OA, Spira ME (2014) Rescue of tau-induced synaptic transmission pathology by paclitaxel. Front Cell Neurosci 8, 34. [PubMed: 24574970]

[49]. Magistretti PJ, Pellerin L (1999) Cellular mechanisms of brain energy metabolism and their relevance to functional brain imaging. Philos Trans R Soc Lond B Biol Sci 354, 1155–1163. [PubMed: 10466143]

[50]. Sokoloff L (1993) Sites and mechanisms of function-related changes in energy metabolism in the nervous system. Dev Neurosci 15, 194–206. [PubMed: 7805571]

[51]. Buchsbaum MS, Simmons AN, DeCastro A, Farid N, Matthews SC (2015) Clusters of low (18)F-fluorodeoxyglucose uptake voxels in combat veterans with traumatic brain injury and post-traumatic stress disorder. J Neurotrauma 32, 1736–1750. [PubMed: 25915799]

[52]. Shinoda J, Asano Y (2017) Disorder of executive function of the brain after head injury and mild traumatic brain injury - neuroimaging and diagnostic criteria for implementation of administrative support in Japan. Neurol Med Chir (Tokyo) 57, 199–209. [PubMed: 28381654]

[53]. Bleeker-Rovers CP, de Kleijn EM, Corstens FH, van der Meer JW, Oyen WJ (2004) Clinical value of FDG PET in patients with fever of unknown origin and patients suspected of focal infection or inflammation. Eur J Nucl Med Mol Imaging 31, 29–37. [PubMed: 14551752]

[54]. Semmler A, Hermann S, Mormann F, Weberpals M, Paxian SA, Okulla T, Schafers M, Kummer MP, Klockgether T, Heneka MT (2008) Sepsis causes neuroinflammation and concomitant decrease of cerebral metabolism. J Neuroinflammation 5, 38. [PubMed: 18793399]

[55]. Dent EW (2017) Of microtubules and memory: Implications for microtubule dynamics in dendrites and spines. Mol Biol Cell 28, 1–8. [PubMed: 28035040]

[56]. Reger MA, Watson GS, Frey WH 2nd, Baker LD, Cholerton B, Keeling ML, Belongia DA, Fishel MA, Plymate SR, Schellenberg GD, Cherrier MM, Craft S (2006) Effects of intranasal insulin on cognition in memory-impaired older adults: Modulation by APOE genotype. Neurobiol Aging 27, 451–458. [PubMed: 15964100]

[57]. Brabazon F, Wilson CM, Jaiswal S, Reed J, Frey WHN, Byrnes KR (2017) Intranasal insulin treatment of an experimental model of moderate traumatic brain injury. J Cereb Blood Flow Metab 37, 3203–3218. [PubMed: 28058996]

[58]. Kurland D, Hong C, Aarabi B, Gerzanich V, Simard JM (2012) Hemorrhagic progression of a contusion after traumatic brain injury: A review. J Neurotrauma 29, 19–31. [PubMed: 21988198]

[59]. Lawrence TP, Pretorius PM, Ezra M, Cadoux-Hudson T, Voets NL (2017) Early detection of cerebral microbleeds following traumatic brain injury using MRI in the hyper-acute phase. Neurosci Lett 655, 143–150. [PubMed: 28663054]

[60]. Watanabe J, Maruya J, Kanemaru Y, Miyauchi T, Nishimaki K (2016) Transient disappearance of microbleeds in the subacute period based on T2*-weighted gradient echo imaging in traumatic brain injury. Acta Neurochir (Wien) 158, 1247–1250. [PubMed: 27106841]

[61]. Toth A, Kovacs N, Tamas V, Kornyei B, Nagy M, Horvath A, Rostas T, Bogner P, Janszky J, Doczi T, Buki A, Schwarcz A (2016) Microbleeds may expand acutely after traumatic brain injury. Neurosci Lett 617, 207–212. [PubMed: 26912192]

[62]. Bruns J Jr, Hauser WA (2003) The epidemiology of traumatic brain injury: A review. Epilepsia 44, 2–10.

[63]. Gornstein E, Schwarz TL (2014) The paradox of paclitaxel neurotoxicity: Mechanisms and unanswered questions. Neuropharmacology 76 Pt A, 175–183. [PubMed: 23978385]

[64]. Kumar H, Mishra G, Sharma AK, Gothwal A, Kesharwani P, Gupta U (2017) Intranasal drug delivery: A non-invasive approach for the better delivery of neurotherapeutics. Pharm Nanotechnol 5, 203–214. [PubMed: 28521670]

[65]. Franklin K, Paxinos G (1997) The Mouse Brain in Stereotaxic Coordinates, Academic Press, San Diego.

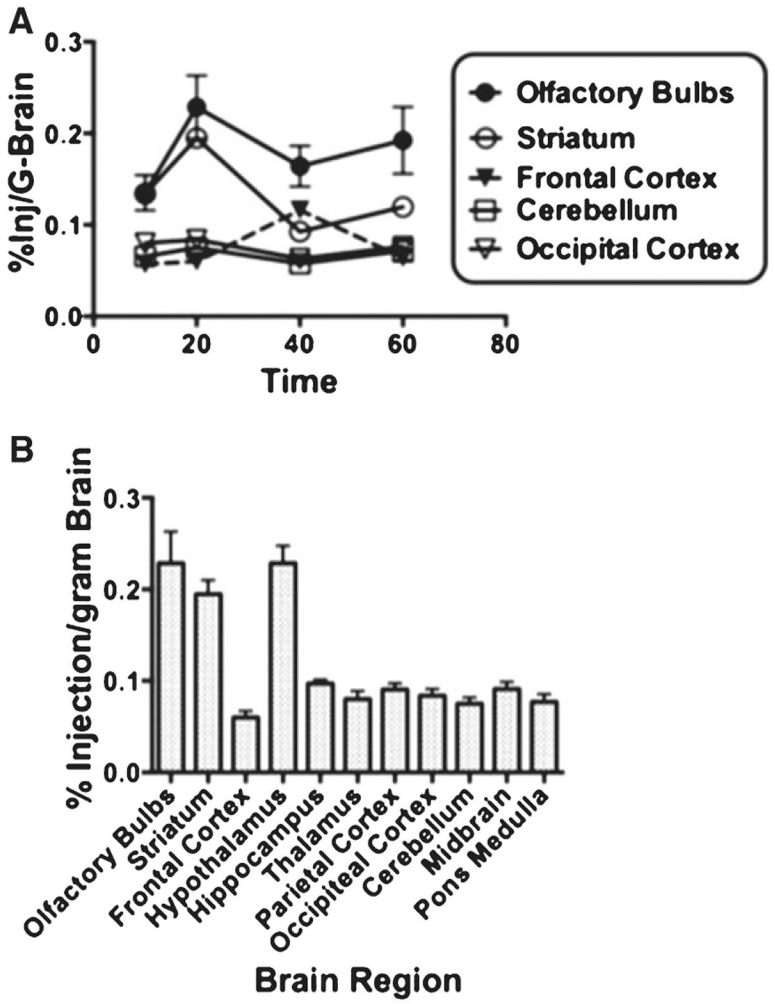

Fig. 1.

Brain distribution of *paclitaxel* after intranasal administration. A) Time-activity curves compare the % Inj/g-brain in five brain regions. Although there are regional differences, tissue concentrations are stable over the 1 hour of sampled time. B) All brain region concentrations of 3H-*paclitaxel* at the 20 min time point from after IN administration show a classic pattern of high olfactory bulb uptake; however, the high striatum and hypothalamus uptake is unique. Results are expressed as the percent of administered dose taken up by a gram of brain region. Error bars indicate standard deviation across the group ($n = 5$).

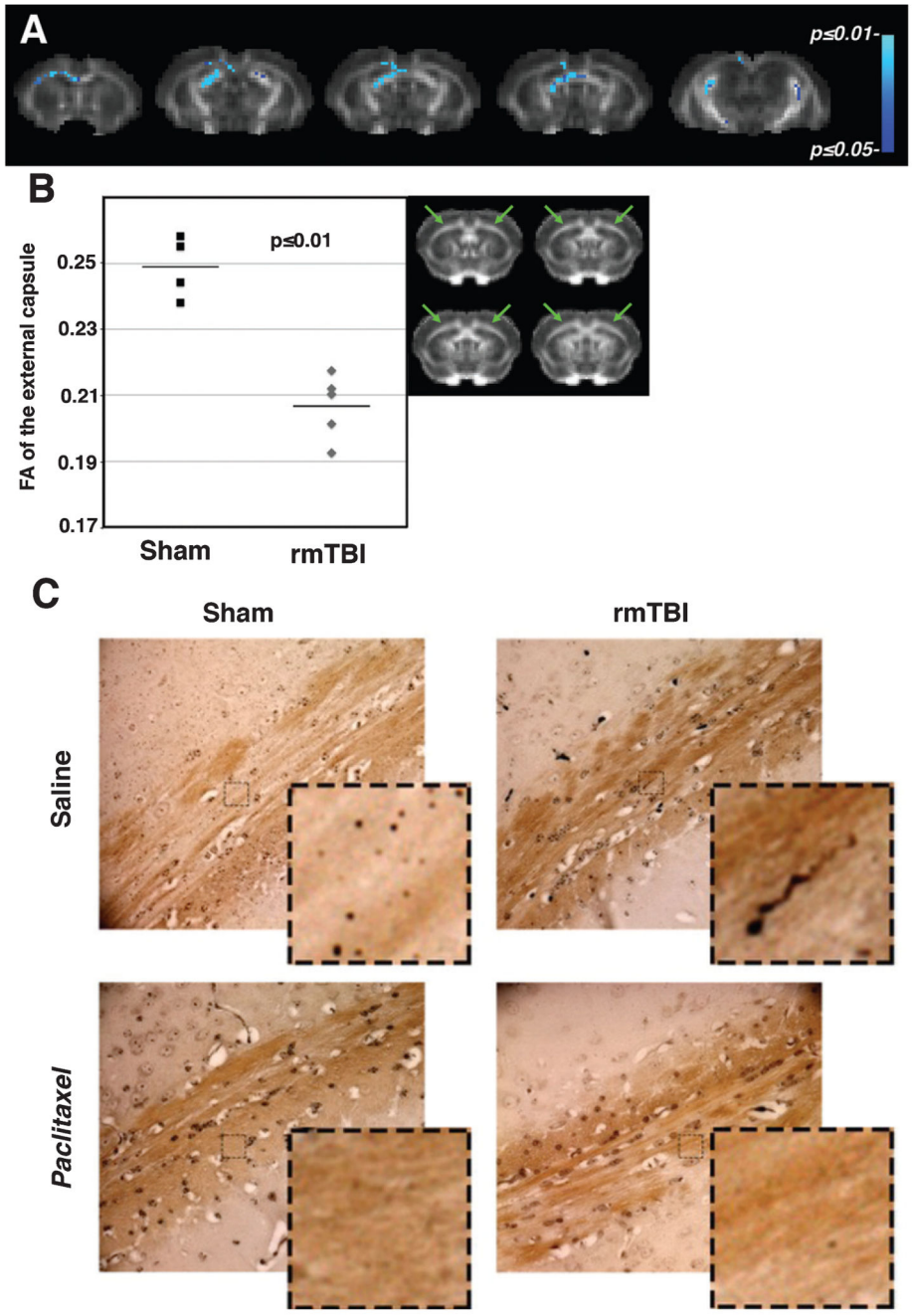

Fig. 2.

White matter injury in the external capsule indicated on DTI and confirmed by silver stain is ameliorated by *paclitaxel.* A) TBSS statistical maps (blue) are superimposed on coronal slices from an FA template brain aligned to the mouse brain atlas for anatomical reference [65]. TBSS indicated that repeat mild brain injury resulted in decreased fractional anisotropy (FA) in diffuse white matter regions throughout the brain, including the external capsule at 4 days after final impact. Color scale bar to the right indicates *p*-values. B) Scatterplot of the manual ROI analysis of the external capsule (location indicated by green arrows), shows that FA was decreased significantly by 17% (0.21 ± 0.01 versus 0.25 ± 0.01, mn ± sd, $p \leq 0.01$)

compared to sham mice. Horizontal line indicates mean. C) Representative samples indicate axonal injury in cortical white matter of the external capsule/alveus by rmTBI as demonstrated by Gallyas silver staining. Mice were perfused for immunohistochemistry at 45 days after rmTBI. Argyrophilic axonal degeneration was found in 5/6 saline-treated but not *paclitaxel*-treated mice (n = 0/5) or sham-*paclitaxel*-treated controls (n = 0/3). A single, unilateral dystrophic axonal bulb was observed in 1/5 sham mice. Insets represent magnifications of boxed areas.

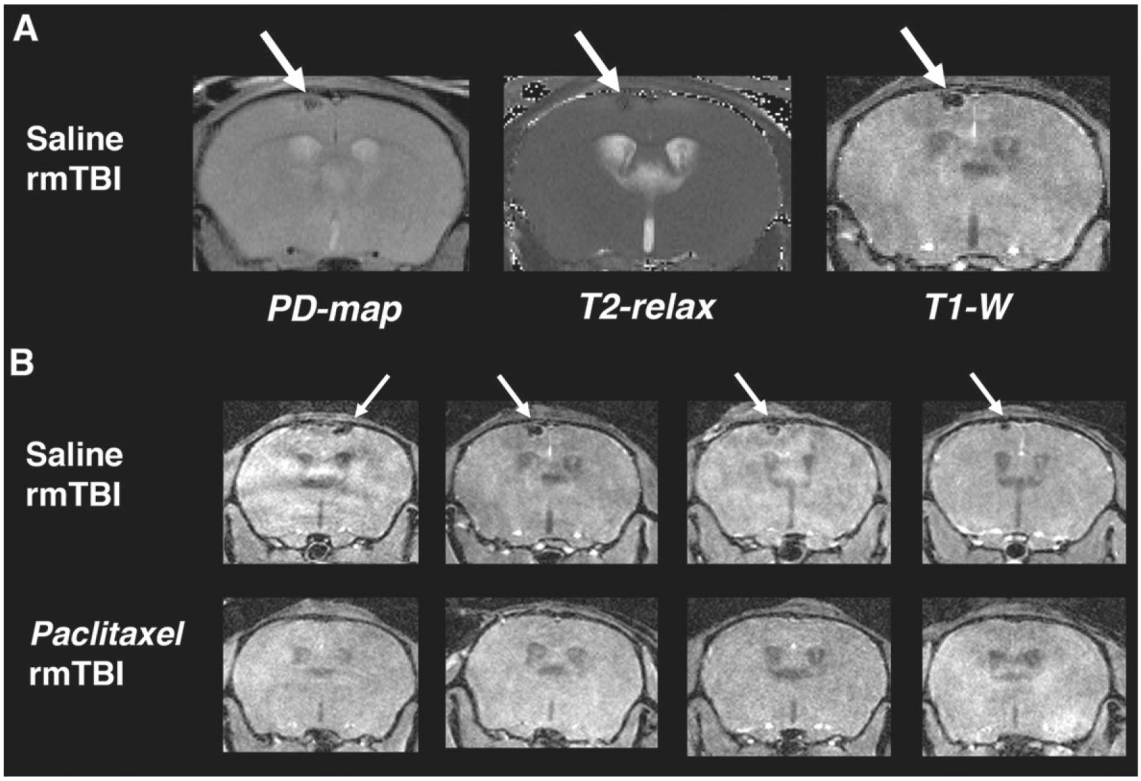

Fig. 3.

Paclitaxel prevents brain lesions associated with rmTBI. MR imaging was acquired at 4 days post-rmTBI to assess injury and response to *paclitaxel* treatment *in vivo.* A) Left to right: Proton Density mapping (PD-map), T2-relaxation quantitative image (T2-relax) and T1-weighted image (T1-W) from the same saline-treated mouse (coronal view). Green arrows indicate a dark spot in the cortex just below the impacted region. Spot is dark in all 3 images indicating a likely tissue strain microbleed. B) T1-W imaging of saline- (top row) and paclitaxel-treated (bottom row) from 4 subjects of each group. 100% (8/8) saline-treated subjects had microbleed lesion at 4 days post injury and 0% (0/6) of the *paclitaxel*-treated showed evidence of the lesion.

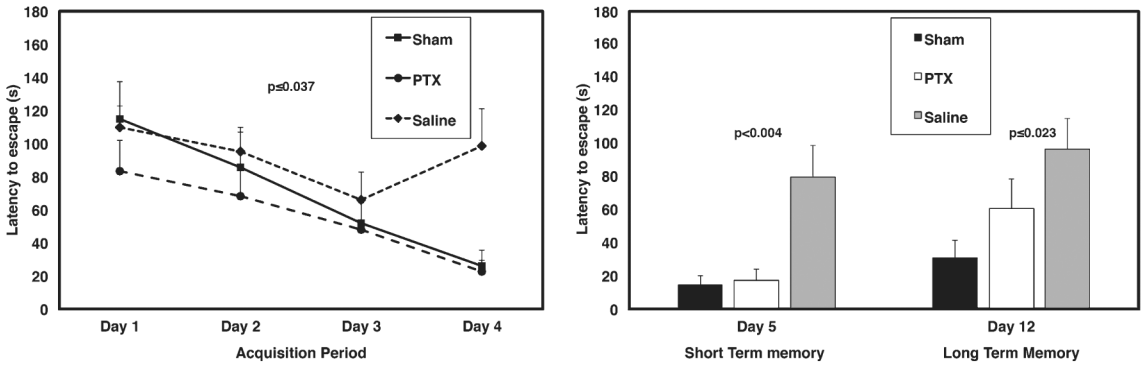

Fig. 4.

Paclitaxel preserves short- and long-term memory. The radial water tread (RWT) maze tests spatial learning and memory. Maze test was administered from Day 10 to 22 post-injury. A) Graph indicates learning/acquisition phase over Days 1–4, where saline-treated rmTBI mice did not learn the maze as compared to sham and PTX-treated rmTBI. *Paclitaxel* (PTX) rmTBI mice learned the maze similar to Sham. B) *Paclitaxel* subjects were significantly improved from saline in both short-term memory (Day 5) as well as long term memory (tested on Day 12).

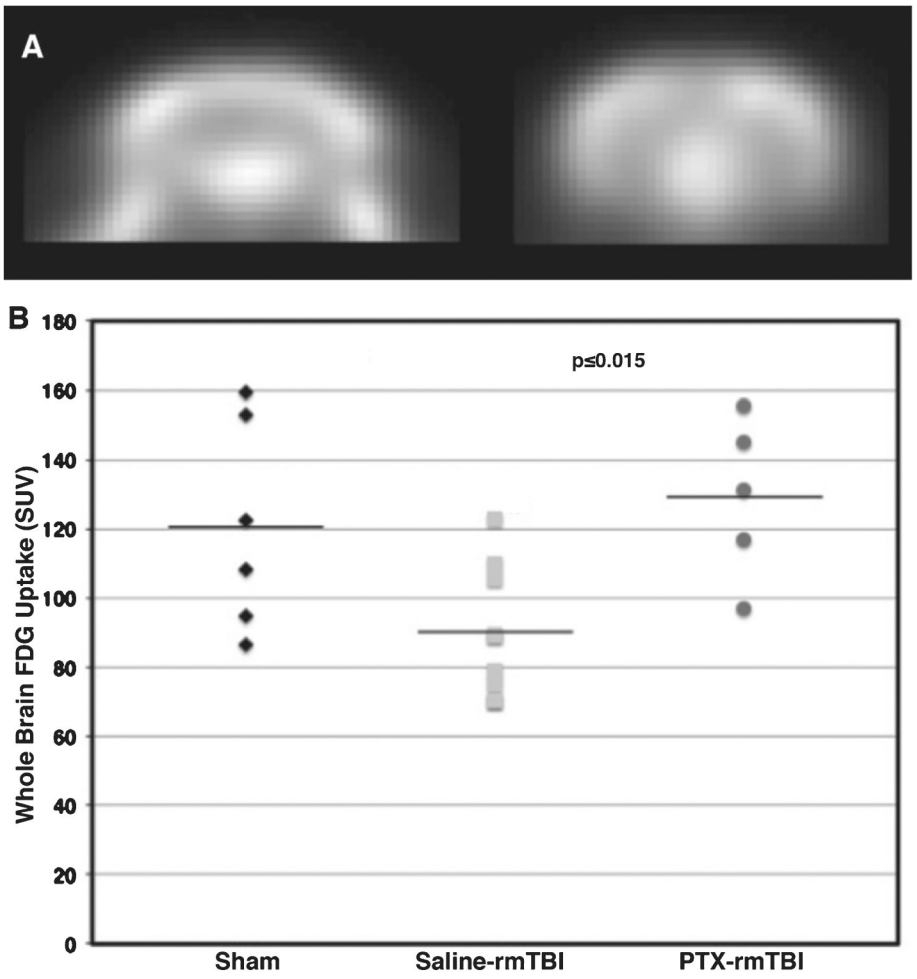

Fig. 5.

Paclitaxel preserves FDG brain uptake. A) Representative mouse brain FDG-PET image (coronal view) from a single sham subject to illustrate image quality. B) Scatterplot of standardized uptake values (SUV) from saline-treated rmTBI mice shows significantly decreased brain FDG uptake at 31 days post injury, which was preserved in mice administered IN *paclitaxel.* Horizontal lines indicate mean.

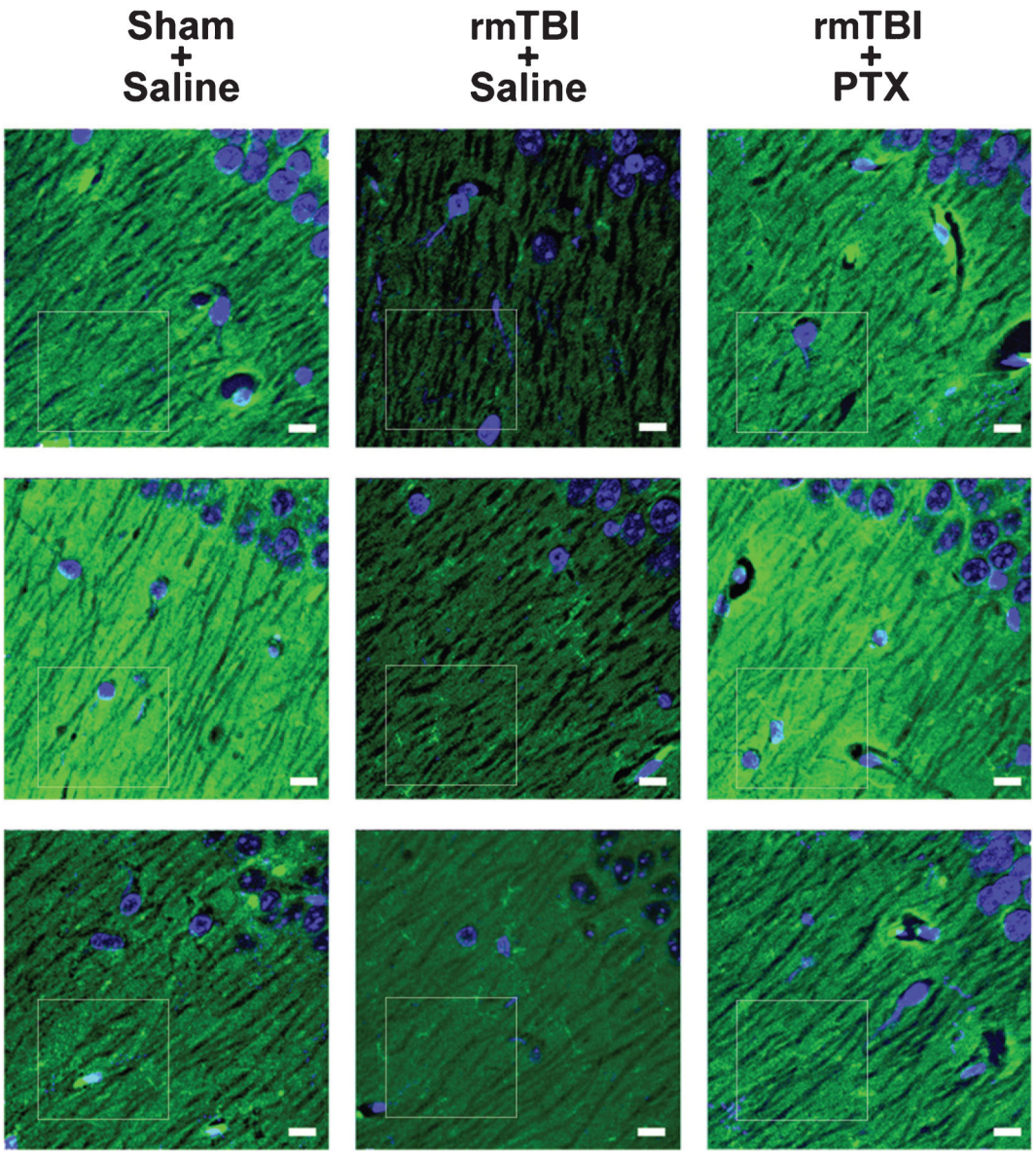

Fig. 6.

Paclitaxel treatment blocks rmTBI-induced loss of postsynaptic density-95 immunoreactivity in hippocampus. Representative PSD-95 (green) expression in CA1 stratum oriens hippocampi. Tissue was counterstained with DAPI (blue) to delineate prominent nuclei of the stratum pyramidale. In saline-treated mice exposed to rmTBI, hippocampal PSD-95 immunofluorescence was reduced as compared to sham or rmTBI *paclitaxel* mice. CA1 (just superior to the dentate lateral horn) is near the location of the Gallyas silver stain from Fig. 2C. Confocal micrographs are from 3 mice in each group. White boxes indicate region of fluorescence analysis. Bars = 10 μm.